Ultralight High-Efficiency Flexible InGaP/(In)GaAs Tandem Solar Cells on Plastic

Davood Shahrjerdi, Stephen W. Bedell, Can Bayram, Cristina C. Lubguban, Keith Fogel, Paul Lauro, John A. Ott, Marinus Hopstaken, Michael Gayness, and Devendra Sadana*

Flexible solar cells are envisioned to open up a myriad of possibilities for enabling new applications in consumer electronics and space satellites.[1–3] Organic and amorphous semiconductors hold a great promise for realizing bendable and light-weight solar cells, largely due to their fairly strong light absorption properties, process temperature compatibility with flexible substrates and potentially inexpensive processing cost.[4–6] However, the poor minority carrier lifetime in these materials, inherent to their highly disordered and defective crystalline structure, inhibit their use for making high efficiency and reliable solar cells. This limitation becomes more pronounced in applications with stringent specifications in terms of the total area and weight of the photovoltaic (PV) module.

Conversely, the exquisite optical and electrical properties of III–V semiconductors permit the fabrication of extremely high-efficiency solar cells exploiting thin III–V layers.[7–9] For example, multijunction III–V solar cells have currently reached ≥36% conversion efficiency at one sun intensity, for which the total thickness of the solar cell structure is ≤10 μm.[10] However, III–V solar cells are conventionally grown on mechanically rigid gallium arsenide (GaAs) and germanium (Ge) substrates that serve as an epitaxial template. Therefore, the release of thin III–V layers from the growth substrate is essential for rendering the solar cell structure flexible. Furthermore, there has been a growing interest in exploiting inverted metamorphic structures to attain higher conversion efficiency, in which the removal of the solar cell structure from the growth substrate is necessary for the proper function of the device.[7,10] It is also important to consider that the use of a viable layer transfer scheme will ideally lead to substantial reduction in material cost by enabling (i) substrate reuse and (ii) thinner solar cell structures with potentially higher conversion efficiency utilizing back reflectors.[11,12]

In order for the widespread adoption of a layer transfer technology, it should offer process simplicity and compatibility with an incumbent solar cell technology, while making it more cost-effective. Recently, there has been an enormous effort to revive the epitaxial layer lift-off (ELO) technique for separating III-V solar cell layers from a GaAs host substrate.[12–17] This technique, in principle, relies on the selective lateral etch of an embedded sacrificial layer – usually an Al-rich AlGaAs layer.[18] From a practical standpoint, an additional apparatus is required to progressively pull the lifted layer away from the host wafer while the sample is immersed in the etch solution – generally concentrated hydrofluoric acid.[14] This is to enhance the inherently slow lateral etch rate of the embedded sacrificial layer and avoid the sudden halt of the etch process. Hence, these practical pitfalls combined with difficulties in handling the free-standing thin layers – particularly film cracking issues during the release process – severely hamper the simplicity and applicability of this method when larger size wafers are used.

We have previously demonstrated the use of our novel layer transfer technique, called controlled spalling for realizing thin-film tandem junction InGaP/(In)GaAs/Ge solar cells rigidly bonded on silicon (Si) handle substrates.[19] This technique works based on the propagation of a spalling mode fracture inside the substrate parallel to the surface, wherein the fracture front is mechanically guided using a flexible handle layer in a controllable manner.[20,21] The equilibrium fracture depth inside the substrate and the final residual strain in the transferred film is engineered by adjusting the intrinsic properties of the stressor layer, which is generally nickel (Ni) owing to its superb fracture toughness. Most notably, the Ni stressor in conjunction with the flexible handle layer provides a robust mechanical support that remarkably facilitates manipulation of very thin layers. The details of the controlled spalling have been described elsewhere.[20,21]

We report here ultralight flexible dual-junction InGaP/(In)GaAs solar cells on plastic with conversion efficiency ≥28% employing the controlled spalling technique. Our solar cells exhibit remarkably high specific power and excellent stability under different bending conditions, thus demonstrating their suitability for applications requiring light-weight and high-efficiency flexible PV. Finally, we demonstrate that the integrity of the entire device structure is maintained during the layer transfer process.

An inverted dual-junction InGaP/(In)GaAs solar cell structure, schematically illustrated in **Figure 1**a, was devised and grown on germanium substrates. In this structure, Ge wafer serves only as an epitaxial template and is not part of the solar cell. However, the growth of an (In)GaAs buffer layer on Ge is necessary to terminate anti-phase boundary defects prior to the growth of the solar cell structure. Because of slight lattice mismatch between GaAs and Ge, it is imperative to incorporate precisely 1% indium in GaAs while growing the buffer layer and the bottom cell in order to avoid the formation of misfit dislocations. It has been previously reported that the misfit dislocations result in the degradation of the open circuit voltage (V_{oc}) without causing an apparent change in the spectral response

D. Shahrjerdi, S. W. Bedell, C. Bayram, C. C. Lubguban, K. Fogel, P. Lauro, J. A. Ott, M. Hopstaken, M. Gayness, D. Sadana
IBM T. J. Watson Research Center
Yorktown Heights, NY 10598
E-mail: davood@us.ibm.com

DOI: 10.1002/aenm.201200827

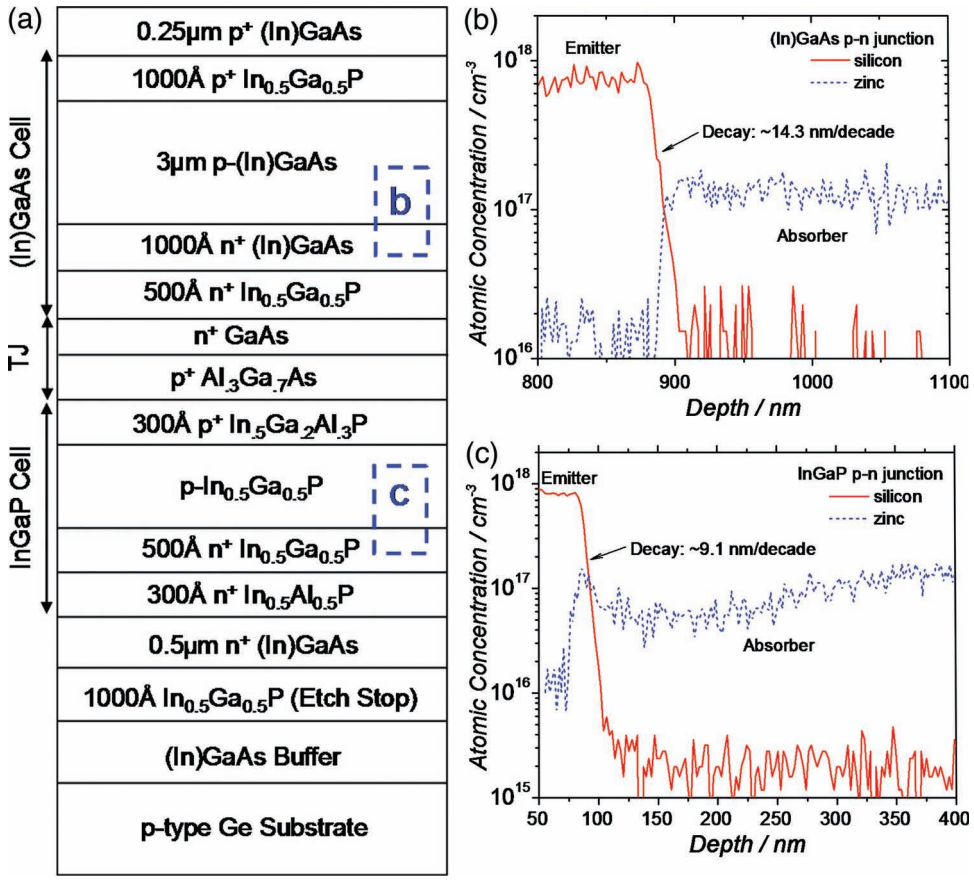

Figure 1. (a) Schematic illustration of the inverted dual-junction InGaP/(In)GaAs tandem solar cell grown on Ge substrates. (b),(c) Depth profiling SIMS results demonstrating the abruptness of the p-n junctions in (In)GaAs and InGaP cells, respectively.

of the GaAs cell.[22] The small indium content of the (In)GaAs layer will however prevent the V_{oc} loss as a result of the misfit dislocation formation, while extending the absorption edge to slightly longer wavelengths due to its smaller bandgap compared to GaAs. Another important growth consideration for dual-junction solar cells is to account for the influence of various growth conditions including growth temperature, growth rate, nucleation layer, and Ge miscut angle on the bandgap of the top cell and the resulting conversion efficiency due to the ordering related effects in InGaP.[23,24] Therefore, the growth conditions were optimized to obtain a bandgap of 1.86 eV for the InGaP absorber layer in the top cell. Furthermore, compared to the upright tandem InGaP/(In)GaAs/Ge solar cells, the p-n junctions in the inverted dual junction structure are subjected to larger thermal budget since the thick absorber layers are grown after the thin emitter layers. Consequently, 10-nm-thick unintentionally doped layers were inserted between the emitter and absorber regions for both the InGaP and (In)GaAs cells to suppress the intermixing of dopants at the junctions during the growth. Figure 1b and c illustrate the secondary ion mass spectrometry (SIMS) depth profiling of dopant atoms at the p-n junctions in the (In)GaAs and InGaP cells respectively, confirming the abruptness of the p-n junctions.

Figure 2a–c schematically depicts our fabrication scheme for realizing flexible high-efficiency solar cells on plastic. First, the controlled spalling was performed at room temperature to separate the top 14 μm of the structure from the Ge growth substrate, wherein the removed surface layers consists of the entire III–V solar cell structure, the buffer layer and ~7 μm of Ge. It is important to note that the integration of the entirety of the elements used for the controlled spalling process into the final PV module is appealing because of strong demands for reducing the final cost of solar cells. Uniquely, in our fabrication scheme, the Ni stressor layer that was used for removing the solar cell structure from the growth wafer simultaneously functions as the back ohmic contact. In addition, a thin polyimide tape was utilized as the flexible handle layer to further serve as the support substrate throughout the device fabrication process owing to its exceptional high-temperature stability. Next, the residual Ge film and the buffer layer were selectively etched to expose the (In)GaAs contact layer. A low-temperature fabrication process (≤200 °C) was devised due to the temperature limitation imposed by the polyimide tape. The fabrication process involves the formation of the lithographically defined front contact grid consisting of Pd/Ge/Au/Ag layers (100 Å/400 Å/1000 Å/3 μm) with a shadowing loss of <2%. The cell area was defined by chemical mesa etch, followed by annealing at 175 °C to form low resistivity ohmic contacts – with specific contact resistance of $\leq 6 \times 10^{-6}$ Ω.cm^2 – to the n$^+$ (In)GaAs contact layer.[25] The cell fabrication was completed by selective removal of the (In)GaAs layer between metal grid contacts followed by the evaporation of a double layer ZnS/MgF_2 antireflection

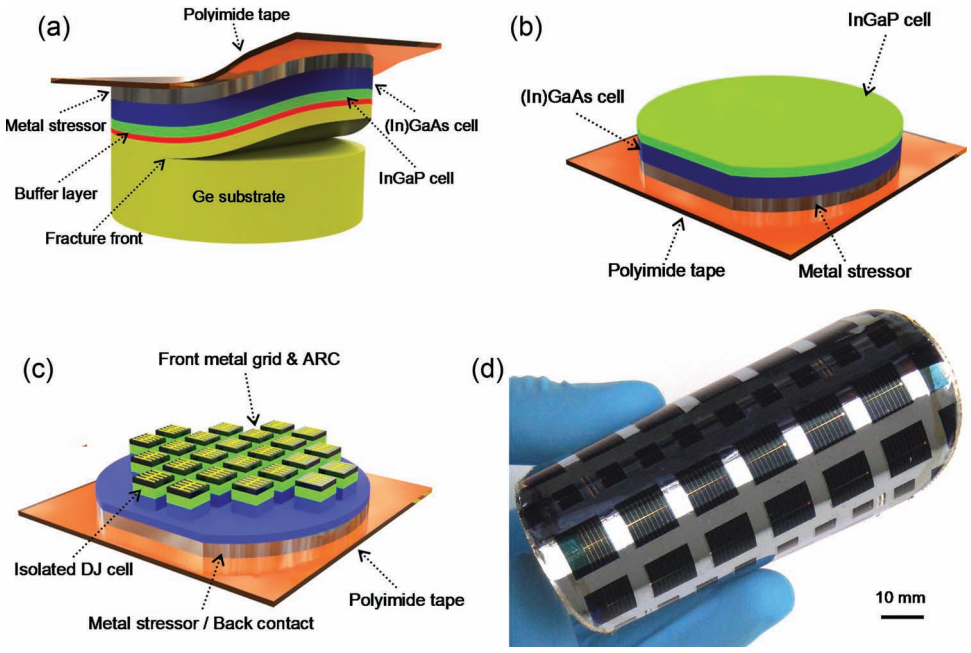

Figure 2. Pictorial representation of the key process steps for making the flexible III–V solar cells involving (a) controlled spalling to separate the solar cell structure from the growth wafer, (b) selective removal of the excess Ge and the buffer layer to expose the solar cell structure, (c) front grid and ARC depositions and cell isolation. (d) Photograph of the final 100-mm-diameter flexible InGaP/(In)GaAs tandem solar cell on plastic.

coating (ARC) (see Experimental Section for more details on the fabrication process). Figure 2d illustrates the photograph of a 100 mm diameter flexible dual-junction InGaP/(In)GaAs solar cells on plastic.

Current matching between the top and bottom cells is imperative for achieving the highest total current in series connection and is obtained by adjusting the thickness of the top InGaP cell.[26] The inset in **Figure 3**a shows the theoretical calculations for the air mass (AM) 1.5 solar spectrum after passing consecutively through ~30 nm InAlP window layer, and an InGaP layer with thickness of 400 and 600 nm, assuming a single pass of the light. The absorption coefficients for the InAlP and InGaP layers were estimated from the equations described by H. Kato *et al.*[27] From these calculations, it was found that ~48.6 and 51.4% of the total absorbed solar spectrum by the dual-junction solar cell are respectively absorbed in the 400 and 600 nm thick top InGaP cells. The remaining photons with an energy ranging from 1.405–1.86 eV are subsequently absorbed by the bottom cell, assuming an infinitely thick (In)GaAs absorber layer. In this work, the thickness of the bottom cell was chosen to be 3 µm in order to allow the absorption of >96% of the incoming photons in a single pass of the light, calculated from the Beer-Lambert law using the absorption coefficient of GaAs.[28] As a result, we have grown and fabricated two flexible dual-junction solar cells (structures A and B) with an InGaP base layer thickness of 400 and 600 nm, respectively. Figure 3a shows the current density-voltage (*J–V*) characteristics of the champion flexible cells for the structures A and B, measured under the simulated AM 1.5 solar spectrum at one sun intensity. As can be seen, the champion cells demonstrate similar conversion efficiency of ~28.1%. In order to obtain further insight about the current matching between the cells, the external quantum efficiency (EQE) of the champion cells were measured (Figure 3b) and the integrated current density of the top and bottom cells was then estimated for each device from its respective EQE curve. The summary of the light *J–V* characteristics for the champion cells and their corresponding EQE analysis are listed in **Table 1**. The EQE analysis indicates that the J_{sc} in the structures A and B is limited by the top InGaP and the bottom (In)GaAs cells, respectively. Additionally, the difference in the total integrated current density of the top and bottom cells suggests that further improvement in J_{sc} can be obtained by tailoring the thickness of the InGaP absorber layer in the range of 400 to 600 nm.

The specific power is considered a key parameter while assessing the suitability of a PV technology for light-weight applications. The specific power of our flexible dual-junction solar cells was calculated to be >1995 W/kg, assuming power output of 28 mW/cm^2 under AM 1.5 solar spectrum. Therefore, this remarkably high specific power makes our flexible PV devices an attractive candidate for light-weight and high-efficiency PV modules. For flexible electronic applications, it is also important to examine the stability and endurance of flexible devices under different bending radii of curvature and repeated bending cycles. Bending tests were performed using circular cylinders with different radii of curvature (from 10 to 20 mm), illustrated as the inset in **Figure 4**a. The V_{oc} of the cells remained unchanged under tensile bending conditions, while the J_{sc} begins to drop as the radius of curvature was reduced, shown in Figure 4a. We surmise that slight change in the reflection properties of the ARC layer is accountable for the observed reduction in J_{sc}, caused by the change of the light path length in the ARC layer over the curved regions. Furthermore, the bending endurance of the flexible dual-junction solar cell was successfully demonstrated up to 1000 cycles at the radius of 10 mm without any noticeable change in device characteristics, shown in Figure 4b.

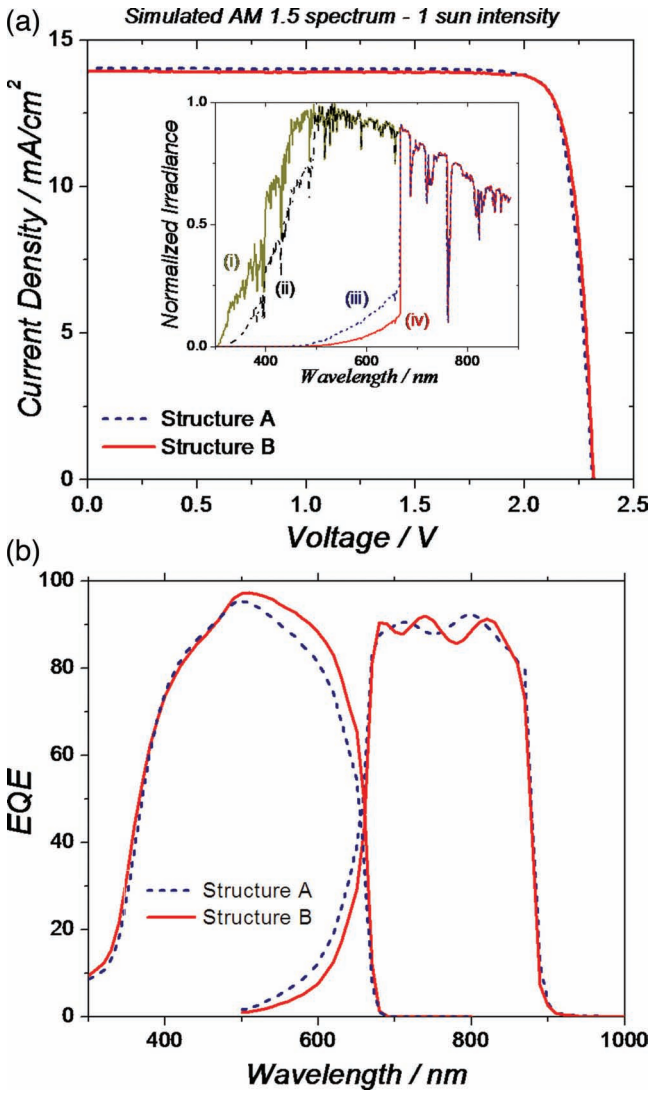

Figure 3. (a) Light *J–V* characteristics of the 1cm × 1 cm champion flexible cells on structures A and B. The inset shows (i) the normalized AM1.5 spectral irradiance after consecutively passing through (ii) 30 nm InAlP layer and InGaP absorber layers with a thickness of (iii) 400 nm and (iv) 600 nm. (b) The corresponding EQE data for the devices in (a), illustrating the spectral response of individual sub cells.

Finally, to elucidate the possible effects of the spalling process on the structural and electrical properties of the solar cells, we have performed extensive material and electrical characterizations. Transmission electron microscopy (TEM)

Table 1. Summary of the light *J–V* and EQE measurements for the champion flexible cells on the samples A and B.

Structure	J_{sc} mA/cm²	V_{oc} mV	FF %	η %	$J_{InGaP\ cell}$[a] mA/cm²	$J_{(In)GaAs\ cell}$[a] mA/cm²
A	14.0	2312	86.8	28.1	14.2	14.8
B	13.9	2313	87.4	28.1	15	14.1

[a] ((Current density of individual sub cells estimated from the EQE data shown in Figure 3b.))

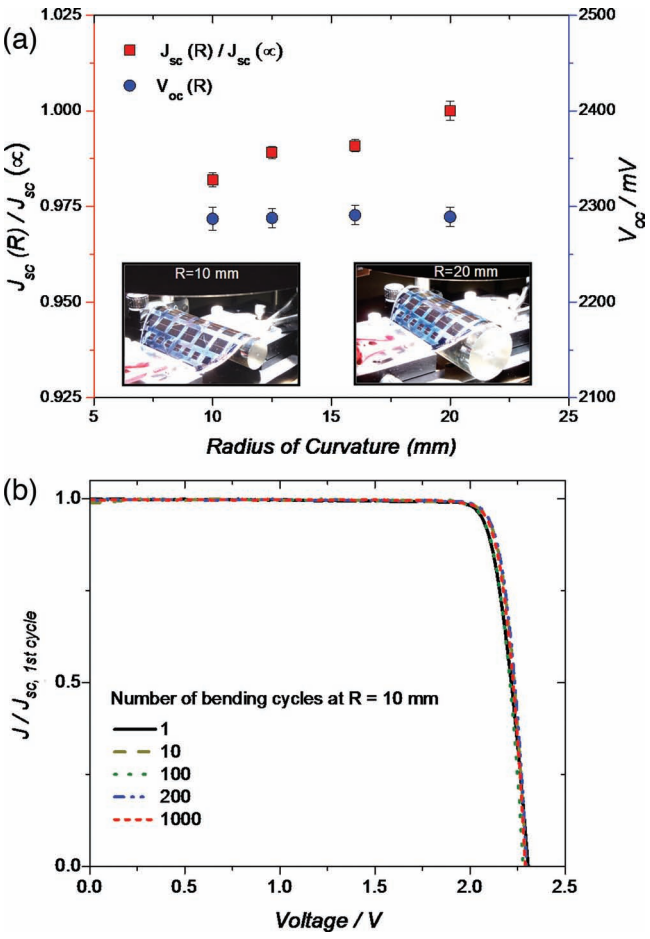

Figure 4. Our flexible solar cells exhibit excellent stability (a) under bending at different radii of curvature and (b) repeated bending up to 1000 cycles.

was used to study the structural integrity of the flexible solar cells after spalling. **Figure 5** illustrates the representative cross-sectional TEM images taken from different parts of the solar cell structure, revealing abrupt interfaces and no clear evidence of defect formation as a result of the spalling process. It is also notable that the electrical characteristics of devices can readily provide important information about vital device parameters over a large span of a sample. In particular, it is possible to verify subtle changes in the intrinsic material properties such as minority carrier lifetime in the absorber layer and surface recombination velocity at different interfaces using various electrical measurements. For example, quantum efficiency measurements can be used as a means to evaluate the front and back surface passivation, tunneling junctions and bulk minority carrier lifetimes in a solar cell structure by analyzing different regions of a quantum efficiency curve. Furthermore, the degradation of material properties as a result of defect formation or channel cracking will directly impact the solar cell dark current, which will result in V_{oc} degradation. To investigate the effect of spalling on the electrical properties of the flexible solar cells, a monitor sample was prepared by bonding an inverted dual-junction solar cell sample on a Si handle wafer using a silver-based conductive epoxy, followed by the chemical

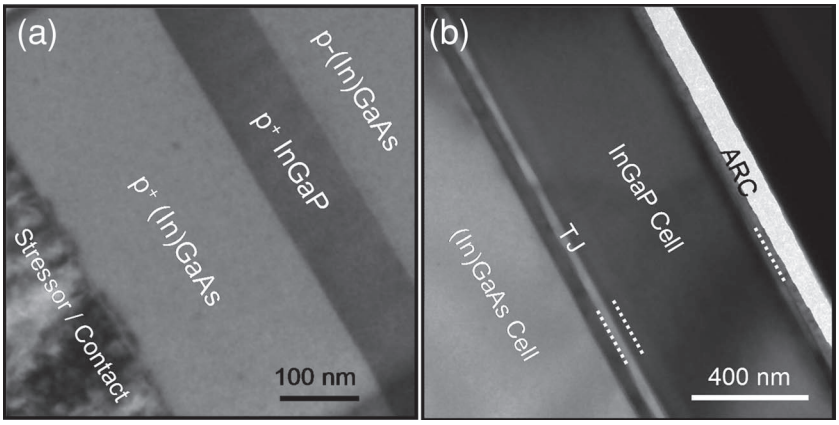

Figure 5. Representative cross-sectional TEM images of the (a) bottom and (b) top portions of a flexible solar cell, indicating the formation of no visible crystalline defects as a result of the spalling process.

removal of the Ge wafer and the (In)GaAs buffer layer to expose the solar cell structure. The bonded sample then underwent similar processing steps as the flexible solar cells. **Figure 6** illustrates the comparison of the light *J–V* characteristics and the spectral responses for the bonded sample and its flexible counterpart prepared using the controlled spalling process. The nearly identical J_{sc} and V_{oc} of the champion cells on both the bonded and flexible samples and their overlapping EQE curves confirm the equivalency of the bonded and flexible samples. The equivalency of the electrical data further suggests that the intrinsic material properties throughout the entire flexible solar cell structure have remained unchanged during the layer transfer process. It should be noted that the slightly lower fill factor of the monitor sample compared to its flexible counterpart is attributed to the degraded electrical properties of the conductive epoxy during the annealing step at 175 °C.

In summary, we have demonstrated light-weight high-efficiency flexible dual-junction InGaP/(In)GaAs solar cells with a conversion efficiency of ≥28% on plastic, using controlled spalling technique. The Ni stressor layer used for the spalling process was integrated in our solar cell structure as the back ohmic contact to allow further reduction of the PV cost. Furthermore, our flexible solar cells can be deployed for applications requiring light-weight PV, owing to their remarkably high specific power, in excess of 1995 W/kg. The stability of the electrical characteristics of the flexible solar cells was demonstrated under different bending conditions and a large number of repeated bending cycles, further highlighting the prospects of these devices for applications in high-performance flexible electronics. Finally, the comparison of the structural and electrical properties of the flexible solar cells with a monitor sample that was prepared by chemical removal of the Ge substrate, revealed the equivalency of the devices.

Experimental Section

Epitaxial growth of the solar cell structures was performed on 100 mm diameter (100) Ge substrates with 6° miscut angle toward [111] using the Veeco's K475 commercial MOCVD reactor at ~640 °C. The InGaP etch stop layer was removed in pure hydrochloric acid. The solar cell mesa etch was done using CH_3-COOH:HNO_3:H_2O (1:1:5) for 6 minutes. The (In)GaAs contact layer was selectively etched in citric acid:H_2O_2 (7:1). The citric acid solution was prepared by dissolving anhydrous citric acid powder in de-ionized water (1 gram: 1 ml). The ZnS and MgF_2 layers were thermally evaporated to a thickness of 54 nm and 92 nm, respectively. The Ge substrate for the monitor sample was fully removed in hydrogen peroxide. The light *J–V* characterization for the solar cells was performed using a Xe-based light source solar simulator. The one sun illumination intensity was calibrated using a Si reference cell, measured by National Renewable Energy Laboratory. The quantum efficiency measurements were performed using QEX10 system. Secondary ion mass spectrometry (SIMS) depth profiles were acquired using a magnetic sector Cameca Wf Ultra instrument equipped with a floating 60° Cs^+ column. Profiles for Si were obtained with a 1.5 keV Cs^+ ion beam, while analyzing negative Si-cluster ions ($AsSi^-$ and PSi^- in $In_xAl_yGa_{1-x-y}As$ and $In_xAl_yGa_{1-x-y}P$ layers, respectively) at high mass resolution. Profiles for

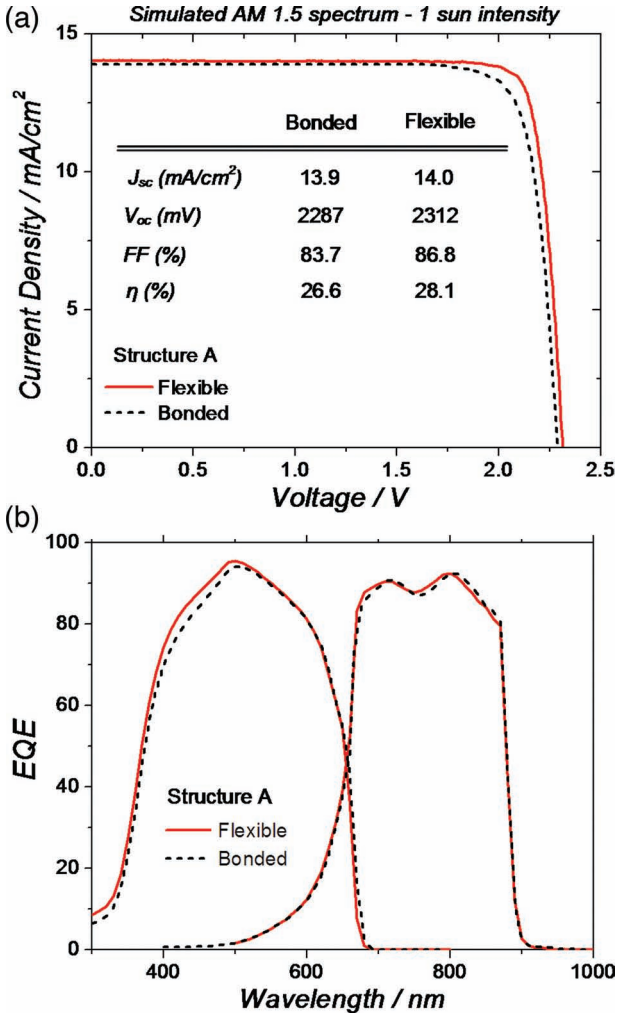

Figure 6. Comparison of the (a) light *J–V* and (b) EQE characteristics of champion cells on the flexible and its counterpart monitor samples reveals the equivalency of the solar cell devices.

Zn were obtained with a 1.5 keV Cs^+ ion beam, while analyzing positive $CsZn^+$ cluster ions. Depth calibration was based on the GaAs erosion rate whereas concentration scales were derived using the appropriate implant standards in different matrices (i.e. GaAs, InGaP).

Acknowledgements

The authors would like to gratefully acknowledge Dr. Ghavam G. Shahidi for his technical guidance and managerial support. This work was performed under a joint development agreement between IBM Research and the King Abdulaziz City for Science & Technology (KACST) in Riyadh, Kingdom of Saudi Arabia. The authors would also like to acknowledge Chris Ebert and Veeco MOCVD team for allowing the use of their MOCVD facility and valuable technical discussions on the material growth.

Received: October 15, 2012
Published online: December 13, 2012

[1] Y. Kishi, H. Inoue, K. Murata, H. Tanaka, S. Kouzuma, M. Morizane, Y. Fukuda, H. Nishiwaki, K. Nakano, A. Takeoka, M. Ohnishi, Y. Kuwano, *Solar Energy Mater.* **1991**, *23*, 312.
[2] M. B. Schubert, J. H. Werner, *Mater. Today* **2006**, *9*, 42.
[3] N. G. Dhere, S. R. Ghongadi, M. B. Pandit, A. H. Jahagirdar, D. Scheiman, *Prog. Photovoltaics* **2002**, *10*, 407.
[4] S. E. Shaheen, C. J. Brabec, N. S. Sariciftci, F. Padinger, T. Fromherz, J. C. Hummelen, *Appl. Phys. Lett.* **2001**, *78*, 841.
[5] F. Kessler, D. Rudmann, *Solar Energy* **2004**, *77*, 685.
[6] B. Rech, H. Wagner, *Appl. Phys. A* **1999**, *69*, 155.
[7] J. F. Geisz, S. Kurtz, M. W. Wanlass, J. S. Ward, A. Duda, D. J. Friedman, J. M. Olson, W. E. McMahon, T. E. Moriarty, J. T. Kiehl, *Appl. Phys. Lett.* **2007**, *91*, 023502.
[8] R. R. King, D. C. Law, K. Edmondson, C. M. Fetzer, R. A. Sherif, G. Kinsey, D. D. Krut, H. L. Cotal, N. H. Karam, in *Proceedings of the Fourth World Conference on Photovoltaic Energy Conversion* **2006**, 760.
[9] G. J. Bauhuis, P. Mulder, E. J. Haverkamp, J. C. C. M. Huijben, J. J. Schermer, *Solar Energy Mater. and Solar Cells* **2009**, *93*, 1488.
[10] T. Takamoto, T. Agui, A. Yoshida, K. Nakaido, H. Juso, K. Sasaki, K. Nakamora, H. Yamaguchi, T. Kodama, H. Washio, M. Imaizumi, M. Takahashi, in *Proceedings of IEEE 35th Photovoltaic Specialist Conference*, Honolulu, HI **2010**, 412.
[11] O. D. Miller, E. Yablonovitch, S. R. Kurtz, *J. Photovoltaics* **2012**, *2*, 303.
[12] B. M. Kayes, H. Nie, R. Twist, S. G. Spruytte, F. Reinhardt, I. C. Kizilyalli, G. S. Higashi, in *Proceedings of IEEE 37th Photovoltaic Specialist Conference*, Seattle **2011**, *4*.
[13] E. Yablonovitch, T. Gmitter, J. P. Harbison, R. Bhat, *Appl. Phys. Lett.* **1987**, *51*, 2222.
[14] J. J. Schermer, P. Mulder, G. J. Bauhuis, M. M. A. J. Voncken, J. van Deelen, E. Haverkamp, P. K. Larsen, *Phys. Stat. Sol. (a)* **2005**, *202*, 501.
[15] K. Lee, K.-T. Shiu, J. D. Zimmerman, C. K. Renshaw, S. R. Forrest, *Appl. Phys. Lett.* **2010**, *97*, 101107.
[16] J. Yoon, S. Jo, I. S. Chun, I. Jung, H.-S. Kim, M. Meitl, E. Menard, X. Li, J. J. Coleman, U. Paik, J. A. Rogers, *Nature Lett.* **2010**, *465*, 329.
[17] R. Tatavarti, A. Wibowo, V. Elarde, F. Tuminello, R. Pastor, T. Giannopoulos, M. Osowski, R. Chan, C. Youtsey, G. Hillier, N. Pan, in *Proceedings of IEEE 37th Photovoltaic Specialist Conference*, Seattle **2011**, 1941.
[18] M. Konagai, M. Sugimoto, T. Takahashi, *J. Cryst. Growth* **1978**, *45*, 277.
[19] D. Shahrjerdi, S. W. Bedell, C. Ebert, C. Bayram, B. Hekmatshoar, K. Fogel, P. Lauro, M. Gaynes, T. Gokmen, J. A. Ott, D. K. Sadana, *Appl. Phys. Lett.* **2012**, *100*, 053901.
[20] S. W. Bedell, D. Shahrjerdi, B. Hekmatshoar, K. Fogel, P. Lauro, J. A. Ott, N. Sosa, D. Sadana, *IEEE J. Photovoltaics* **2012**, *2*, 141.
[21] S. W. Bedell, D. Shahrjerdi, K. Fogel, P. Lauro, B. Hekmatshoar, N. Li, C. Bayram, J. A. Ott, D. K. Sadana, *Electrochem. Soc. Trans.*, In press.
[22] T. Takamoto, M. Kaneiwa, M. Imaizumi, M. Yamaguchi, *Prog. Photovoltaics* **2005**, *13*, 495.
[23] T. Suzuki, A. Gomoyo, *J. Cryst. Growth* **1990**, *99*, 60.
[24] S. R. Kurtz, J. M. Olson, D. J. Friedman, A. E. Kibbler, S. Asher, *J. Elec. Mater.* **1994**, *23*, 431.
[25] L. C. Wang, P. H. Hao, B. J. Wu, *Appl. Phys. Lett.* **1995**, *67*, 509.
[26] S. R. Kurtz, P. Faine, J. M. Olson, *J. Appl. Phys.* **1990**, *68*, 1890.
[27] H. Kato, S. Adachi, H. Nakanishi, K. Ohtsuka, *Jpn. J. Appl. Phys.* **1994**, *33*, 186.
[28] H. C. Casey, D. D. Sell, K. W. Wecht, *J. Appl. Phys.* **1975**, *46*, 250.